Journal of Catalysis **186,** 147–159 (1999)
Article ID jcat.1999.2528, available online at http://www.idealibrary.com on IDEAL®

Modified Tin(IV) Oxide (M/SnO_2 M = Cr, La, Pr, Nd, Sm, Gd) Catalysts for the Oxidation of Carbon Monoxide and Propane

Philip G. Harrison,[1] Craig Bailey, and Wan Azelee[2]

School of Chemistry, University of Nottingham, University Park, Nottingham NG7 2RD, UK

Received January 6, 1999; revised March 19, 1999; accepted April 7, 1999

Materials formed by the incorporation of rare earth cations (M = La, Pr, Nd, Sm, Gd) into tin(IV) oxide using coprecipitation methods show no significant enhancement of catalytic activity toward the oxidation of carbon monoxide or propane over that of tin(IV) oxide itself. For chromium-promoted tin(IV) oxide catalysts, the temperature by which complete conversion of carbon monoxide and propane occurs is dependent on both the Cr : Sn atom ratio in the catalyst and the preparative route by which the chromium is incorporated into the catalyst. As prepared all the materials are hydrous gels comprising very small (<10 nm) particles of tin(IV) oxide over which the modifying metal component appears to be dispersed uniformly. Chromium(VI) oxyanions of the types CrO_4^{2-}, $Cr_2O_7^{2-}$, and $Cr_3O_{10}^{2-}$ are sorbed on to the surface of the tin(IV) oxide particles in the freshly prepared material derived from aqueous CrO_3 and tin(IV) oxide gel. Prior to calcination the materials are microporous, but significant changes in specific surface area, pore volume, and pore size occur at temperature >673 K. Powder X-ray diffraction and electron microscopy confirm the formation of Cr_2O_3 on calcination at 1273 K.

Key Words: **tin(IV) oxide; chromium; rare earth; CO oxidation; propane oxidation; pore texture; XRD; TEM.**

INTRODUCTION

The control of noxious emissions resulting from the combustion of fossil fuels as well as from other industrial activities is one of the most immediate and compelling problems faced by nearly every country in the world. The levels of pollutants from automobiles, carbon monoxide (CO), hydrocarbons (HCs), and nitrogen oxides (NO_x), are the subject of ever increasingly stringent legislation controlling the maximum permitted levels of emissions of each substance (1, 2). Platinum group catalysts currently represent the state-of-the-art in internal combustion engine emission technology. However, there are significant advantages to be gained from the development of nonnoble metal exhaust emission catalysts not the least of which are the price, strategic importance, and low availability of the platinum group metals.

Although tin(IV) oxide exhibits redox catalytic properties in its own right, these may be modified substantially by the incorporation of heteroelements (3). Such elements include copper, palladium, chromium, and antimony (for total oxidation of carbon monoxide and hydrocarbons), antimony, bismuth, molydenum, and vanadium (for the partial oxidation and ammoxidation of hydrocarbons), and phosphorus and bismuth (for oxidative coupling and oxidative dehydrogenation). Tin oxide-based materials have been known for a long time to have good activity toward the CO/O_2 and CO/NO reactions (4–10), and we have previously reported in the patent literature the efficacy of copper- and chromium-promoted tin(IV) oxide as three-way emission control catalysts (11). These data show that the performance of such catalysts is similar to a Pt/Al_2O_3 catalyst for CO and HC oxidation.

Little is known concerning the constitution of these catalyst materials, the chemistry involved in their preparation, or the surface speciation/reaction mechanisms involved in the catalytic processes. In this paper we report more fully on the activity of chromium promoted tin(IV) oxide catalysts toward the oxidation of carbon monoxide and propane and compare these data with materials derived by the incorporation of lanthanide metal cations into tin(IV) oxide. In addition in an attempt to probe the fundamental reasons for the differences in catalytic behavior, we report initial data concerning the physical and chemical nature of both types of material.

EXPERIMENTAL

Catalyst Preparation

Preparation of Ln(III)/SnO_2 (Ln = La, Pr, Nd, Sm, Gd) Catalysts

Composite lanthanum(III)/tin(IV) oxide materials (Ln : Sn atomic ratio 1 : 10) were prepared by coprecipitation of the hydrous gel. To a vigourously stirred cold solution

[1] To whom correspondence should be addressed.

[2] Present address: Department of Chemistry, Faculty of Science, University Technology Malaysia, Skudai, Locked Beg 791, 80990 Johor Bahru, Malaysia.

0021-9517/99 $30.00

containing ca. 0.1 M tin(IV) chloride (75 g, 33.7 cm^3, 0.288 mol) and lanthanum(III) nitrate hexahydrate (12.467 g, 0.029 mol) in triply distilled water (ca. 500 cm^3) was added concentrated aqueous ammonia solution (Analar, 33%, w/w) to a final pH of 4. The resultant gelatinous precipitate was washed until chloride ion free by repeated centrifuging and redispersing in triply distilled water (negative chloride test using silver nitrate solution). The solid gel was then allowed to air dry at 333 K. At this point the precipitate was of a granular appearance, and approximately 1/10th of its initial volume. These large granules were then broken down by pouring triply distilled water over them. The granules were then washed in nitric acid (Fisons Analar grade diluted with triply distilled water) and then washed to a pH of 4 with triply distilled water followed by air drying at 333 K for 24 h to give a colorless gel. Analogous Pr(III) (greenish gel), Nd(III) (yellowish gel), Sm(III) (purple gel), and Gd(III) (colorless gel) composite oxide materials were prepared by a similar procedure.

Preparation of Cr(VI)/SnO_2 Catalysts

a. Gel impregnation route. Tin(IV) oxide gel (1.00 g), obtained by the hydrolysis of aqueous solution of tin(IV) chloride, was impregnated using aqueous solutions of chromium(VI) oxide in triply distilled water by refluxing at 343 K for 16 h. The yellow powders produced were filtered off and dried at 373 K for 2 h. The Cr : Sn atomic ratio in the products ranged from 0.047 to 0.309.

b. Sol–gel route. An aqueous tin(IV) oxide sol was first prepared by centrifuging hydrated tin(IV) oxide (metastannic acid slop, Keeling and Walker Ltd.) (200 ml) and collecting the resultant solid. Dilute ammonium hydroxide was added until the pH had risen to 10 and the resultant suspension centrifuged again and the solid washed with distilled water. This procedure was repeated another four or five times. Peptization was accomplished using either *N*-butylamine or choline added dropwise with stirring until the mixture became clear. The resulting sol was diluted with distilled water to give a final concentration of ca. 350 g L^{-1}.

To prepare Cr(VI)/SnO_2 catalyst materials, the appropriate amount of a 2 M chromic acid solution was added to a 5-ml aliquot of the sol. The mixture was dried at 343 K in an oven and then calcined at 673 K for 1 h. It was found that addition of chromic acid solution to the sol caused some gelation, so stirring was necessary to homogenize the mixture. The Cr : Sn atomic ratio in the products ranged from 0.063 to 0.744.

Preparation of Cr(III)/SnO_2 Catalysts

These were prepared by mixing the tin(IV) oxide sol with a chromia sol (AERE Harwell). The mixture was stirred, dried down at 343 K, and then calcined at 673 K for 1 h. The Cr : Sn atomic ratio in the products ranged from 0.062 to 0.817.

Physical Measurements

Gas adsorption isotherms were obtained using a custom made apparatus, X-ray diffraction data using a Philips PW 1710 diffractometer (Cu$K\alpha$ radiation $\lambda = 1.54060$ Å), transmission electron microscopy, and corresponding electron diffraction was performed on a Jeol FX III instrument operating at an accelerating voltage of 200 kV, infrared spectra were obtained using Nicolet 20SXC spectrometer, Raman spectra were recorded using a Perkin-Elmer 2000 NIR FT-Raman spectrometer equipped with a Nd^{3+}-YAG laser. Raman spectra were recorded at a low laser intensity of ~100 mV cm^{-2}, in order not to induce any alterations on the surface of the catalyst materials examined. Samples for infrared and Raman examination were calcined at the appropriate temperature and allowed to cool and stored under dry air. Elemental analysis data for tin and chromium were obtained by atomic absorption.

Catalysis Measurements

Catalytic conversion data for the oxidation of carbon monoxide and propane were obtained using a custom built horizontal geometry continuous flow microreactor. The furnace consisted of a stainless steel tube surrounded by a cylindrical stainless steel heating block. The sample tube, which sits inside the stainless steel tube, is made of pyrex glass 1 cm in diameter with a glass sinter in the middle. The catalyst sample was packed on the inlet side of the sinter, supported by dry silica gel pellets, and held in place with glass wool. The outlet side of the sinter was packed with dry silica gel pellets also held in place with glass wool. Catalyst samples were sieved to a particle size range of 38–63 μm, and diluted with silica gel of particle size 100 μm. 0.5 g samples of catalyst were used for carbon monoxide conversions and 2.0 g samples for propane conversions. Catalyst samples were activated by preheating *in situ* in the microreactor at 573 K for 2 h under a flow of air and then allowed to cool also under a flow of air. Catalyst temperatures were measured using a thermocouple located as close to the catalyst as possible. Gas flows were controlled by mass flow controllers, and concentrations of gas phase components were measured using precise integration of characteristic infrared peaks. Compositions of the imput gas mixtures were 5.00% CO, 20.00% O_2, and 75.00% N_2, and 0.78% propane, 20.84% O_2, and 78.38% N_2. An overall flow rate of 100 ml min^{-1} was used for both mixtures corresponding to a space velocities of ca. 18,000 h^{-1} (for CO oxidation) and ca. 4500 h^{-1} (for propane oxidation). Comparative data for commercial 1% Pt/alumina powder (Ventron Alfa Products) were obtained in the same way. The effect of aging was examined by exposing the sol–gel derived Cr(VI)/SnO_2

(Cr : Sn 0.45) catalyst to heat treatment in air at 903 K for 21 h prior to determining CO and propane conversions over a 0.05-g sample as above.

RESULTS

The Catalytic Oxidation of Carbon Monoxide and Propane

Percentage conversion versus temperature plots for the oxidation of carbon monoxide and propane over SnO_2 and the Ln(III)/SnO_2 (Ln = La, Pr, Nd, Sm, Gd) catalysts are shown in Fig. 1. Incorporation of lanthanide cations into tin(IV) oxide gel has little effect on the activity toward the catalytic oxidation of carbon monoxide, essentially irrespective of the particular lanthanide, with complete conversion occuring by 560–575 K (cf. 615 K for SnO_2). Over the same series of catalysts, catalytic oxidation of propane is not complete until ca. 740–750 K, although light-off occurs at temperatures <400 K, behavior which again is very similar to that of SnO_2 itself. The Sm/SnO_2 catalyst is rather different in behavior from the others in that almost 40% conversion occurs by 370 K which remains steady until ca. 540 K before conversion again increases. Light-off temperatures are <373 K except for the Nd(III)/SnO_2 catalyst, which lights off at 423 K.

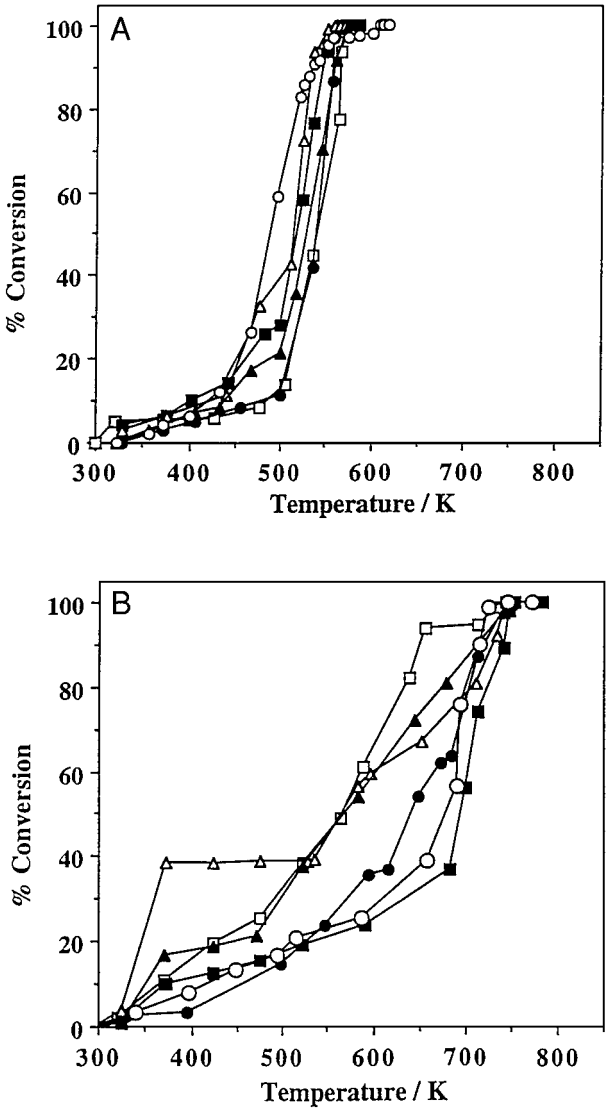

FIG. 1. Percentage conversion versus temperature plots for (A) the oxidation of carbon monoxide and (B) the oxidation of propane over La(III)/SnO_2 (❑), Pr(III)/SnO_2 (■), Nd(III)/SnO_2 (●), Sm(III)/SnO_2 (△), Gd(III)/SnO_2 (▲), and SnO_2 (○).

The temperature by which complete conversion of carbon monoxide and propane occurs is dependent on both the Cr : Sn atom ratio in the catalyst and also on the preparative route by which the chromium is incorporated into the catalyst (Fig. 2). Cr(III)/SnO_2 catalysts are rather insensitive to the Cr : Sn ratio, with $T(100)$ values for conversion (minimum temperature required for complete conversion) of carbon monoxide and propane falling in the ranges 573–613 K and 583–653 K, respectively, both showing rather shallow minima at a Cr : Sn ratio of 0.6. Catalysts obtained using chromium(VI) sources exhibit much more dramatic effects. Catalysts prepared by the sol–gel route exhibit distinct minima for $T(100)$ temperatures for the conversion of both carbon monoxide and propane (at Cr : Sn ratios of ca. 0.4 and 0.45, respectively). The minimum for carbon monoxide is especially clear. Interestingly, it is the catalyst obtained by the impregnation of tin(IV) oxide gel which exhibits both the sharpest minima for both carbon monoxide and propane and at the lowest Cr : Sn ratio (0.15). At this ratio 100% conversion of carbon monoxide occurs at 507 K and conversion of propane at 563 K, compared with lowest $T(100)$ values for the sol–gel derived catalyst of 513 K for carbon monoxide and 553 K for propane.

In spite of the large variation of $T(100)$ values, the percentage conversion versus temperature profiles for the conversion of carbon monoxide are similar in form, with a rapid increase in activity from light-off to 100% conversion over a very narrow temperature range. A typical profile for the sol–gel derived Cr(VI)/SnO_2 (Cr : Sn 0.45) catalyst is shown in Fig. 3 together with the profile of a commercial Pt/Al_2O_3 catalyst, which exhibits a somewhat lower $T(100)$ value of 473 K. Aging at 903 K for 21 h has a marked deleterious effect upon the conversion profile increasing the light-off temperature to ca. 500 K, decreasing the slope of the profile, and attaining only ca. 80% conversion by 820 K (Fig. 3).

Analogous data for the conversion of propane are shown in Fig. 4. While the performance of the sol–gel derived Cr(VI)/SnO_2 (Cr : Sn 0.45) catalyst is quite similar to that of the commercial Pt/Al_2O_3 catalyst for the oxidation of carbon monoxide, it is substantially superior for the catalytic oxidation of propane achieving 100% conversion at 553 K compared to the $T(100)$ temperature for the commercial Pt/Al_2O_3 catalyst of ca. 700 K. As for CO oxidation,

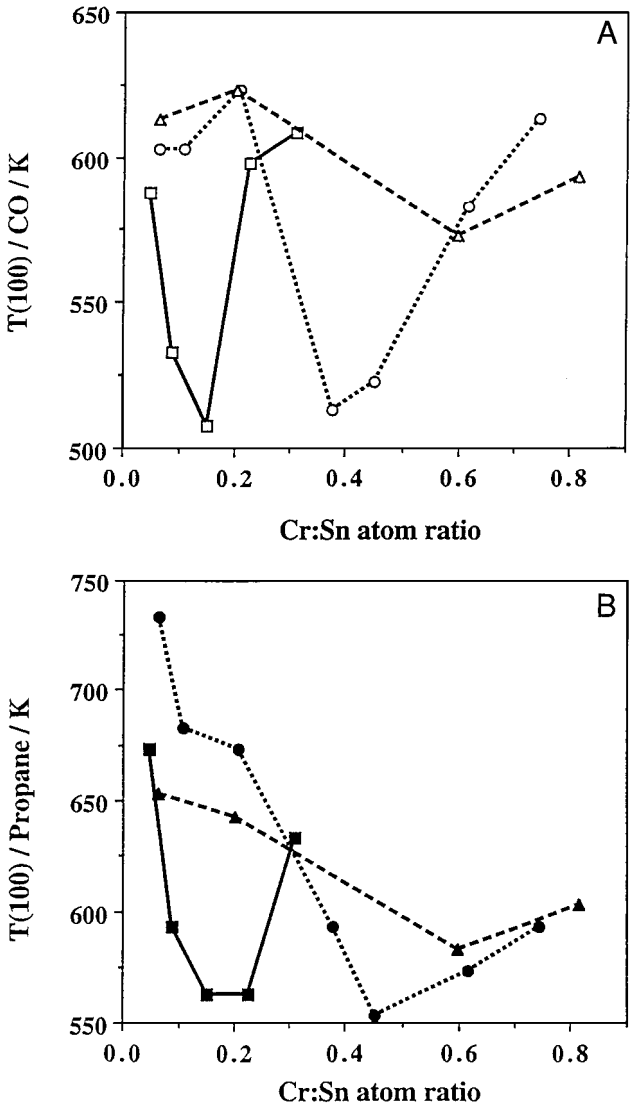

FIG. 2. Plots of minimum temperature required for complete conversion of carbon monoxide (A, white symbols) and propane (B, black symbols) versus the Cr : Sn atomic ratio in Cr(VI)/SnO_2 catalysts prepared by the gel impregnation (■, ❑) and sol–gel (●, ○) routes and Cr(III)/SnO_2 catalysts (▲, △).

accelerated aging at 903 K for 21 h moves the percentage conversion versus temperature profile to higher temperatures, but even then the profile is almost superimposeable on that for the commercial Pt/Al_2O_3 catalyst; i.e., the aged Cr(VI)/SnO_2 catalyst performs as well as the Pt/Al_2O_3 catalyst after similar aging treatments.

Nature of the Catalysts

Powder X-Ray Diffraction

Powder X-ray diffractograms were recorded for the Ln(III)/SnO_2 (Ln = La, Pr, Nd, Sm, Gd) catalyst materials after calcination at various temperatures up to 1373 K.

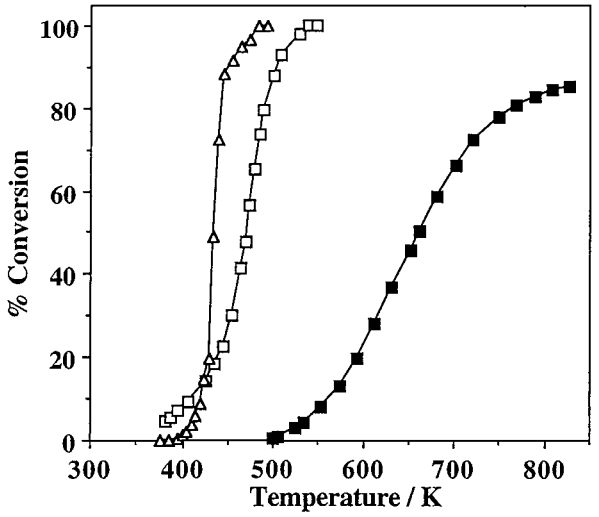

FIG. 3. Percentage conversion versus temperature plots for the oxidation of carbon monoxide over the Cr(VI)/SnO_2 (Cr : Sn 0.45) catalyst after activation at 573 K (❑) and after aging (■) compared with a commercial Pt/Al_2O_3 catalyst (△).

All diffractograms were similar up to calcination temperatures of 1073 K, and distinct differences are only observed at calcination temperatures of 1273 K and above.

Prior to calcination (after drying at 333 K) all the materials exhibited only the four very broad bands characteristic of very small particulate SnO_2. No other bands are observed. However, in some cases (Ln = La, Sm, Gd) weak bands due to cubic Ln_2O_3 phases are observed when a calcination temperature of 873–1073 K is reached. In the case of Ln = Gd, Gd_2O_3 may be formed at lower calcination temperatures. Besides the sintering of the SnO_2

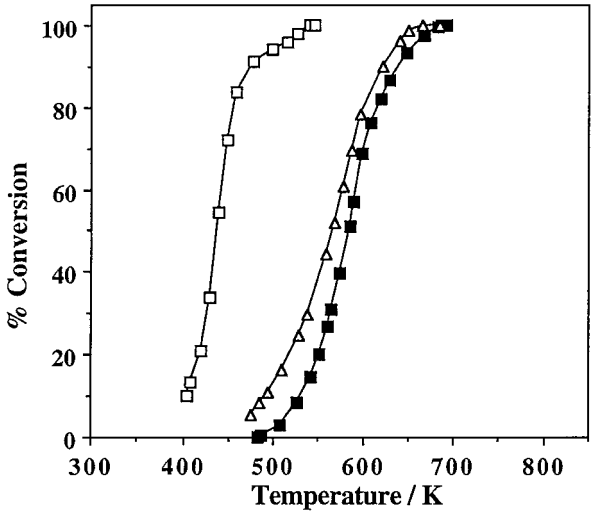

FIG. 4. Percentage conversion versus temperature plots for the oxidation of propane over the Cr(VI)/SnO_2 (Cr : Sn 0.45) catalyst after activation at 573 K (❑) and after aging (■) compared with a commercial Pt/Al_2O_3 catalyst (△).

TABLE 1

Average Particle Size (nm) Calculated from X-Ray Diffraction Peaks Widths for Ln(III)/SnO_2 Catalyst Materials

Catalyst	Phase	Calcination temperature (K)						
		333	573	673	873	1073	1273	1373
SnO_2	SnO_2	10				82	136	208
La(III)/SnO_2	SnO_2				16	22	88	408
	La_2O_3					12	39	62
	$Sn_2La_2O_7$						59	138
Pr(III)/SnO_2	SnO_2	10	12		12	27	32	415
	$Sn_2Pr_2O_7$						103	137
Sm(III)/SnO_2	SnO_2		10	13	22		83	138
	$Sn_2Sm_2O_7$						85	411
Nd(III)/SnO_2	SnO_2			15	22	27	82	147
	$Sn_2Nd_2O_7$						65	436
Gd(III)/SnO_2	SnO_2		10	15		38	415	420
	Gd_2O_3					24	83	91
	$Sn_2Gd_2O_7$						51	455

phase, the major change observed upon increase in calcination temperature is the formation in all the materials of the cubic ternary oxide $Sn_2Ln_2O_7$ phases at temperatures $\geq$1273 K. For $Sn_2La_2O_7$ the unit cell dimension *a* was calculated (12) to be 10.7074 Å, close to the reported (13) value of 10.7020 Å.

Particle size measurements deduced from X-ray line broadening for the Ln(III)/SnO_2 (Ln, La, Pr, Nd, Sm, Gd) catalysts materials are collected in Table 1. All exhibited very similar behavior with respect to thermal treatment. Initially particle sizes of the SnO_2 component are ca. 10 nm and increase very little until ca. >1073 K when a sharp increase takes place, except for Ln = Pr. For the latter material the size of the SnO_2 particles remains relatively small even at 1273 K, but rapid sintering occurs thereafter. Particles of the ternary phases $Sn_2Ln_2O_7$, detected at calcination temperatures $\geq$1273 K, are of a broadly comparable size to the SnO_2 particles. Thus, it would appear that the incorporation of rare earth(III) cations in tin(IV) oxide catalyst materials reduces the tendency toward sintering, allowing particles of SnO_2 to remain relatively small at temperatures in excess of 1073 K.

Powder X-ray diffraction data was obtained only for the Cr(VI)/SnO_2 catalysts obtained by the gel impregnation route, and representative diffractograms for the material with Cr : Sn 0.048 calcined at various temperatures are shown in Fig. 5a with diffractograms of different chromium loadings after calcination at 1273 K (Fig. 5b).

Prior to calcination, all ratios of the Cr(VI)/SnO_2 catalyst materials studied exhibit diffractograms comprising the four characteristic very broad bands due to very small particulate SnO_2. No bands are observed due to other constituents, indicating that they are amorphous in nature. On heating there is a distinct sharpening and increase in intensity of the peaks indicating an increasing crystallinity of the SnO_2 phase, and no other phases are observed even after heating at 873 K. For samples with loadings of Cr : Sn $\leq$ 0.048, no crystalline phase containing chromium could be observed, even after calcination, presumably due to the relatively low level of chromium in this material (Fig. 5b). As such it is unlikely that any crystalline mixed phase would be detected. Particle size measurements deduced from line broadening show that the tin(IV) oxide particle size is insensitive to the level of chromium loading, particles being somewhat larger (11.7 nm) than for the Ln/SnO_2 materials prior to calcination. Sizes increase only ca. threefold by 873 K, but a very sharp increase takes place after calcination at 1273 K (Table 2).

Peaks characteristic of crystalline Cr_2O_3 appear after calcination of the Cr(VI)/SnO_2 (Cr : Sn 0.054) material at 1273 K (Fig. 5a) (lit. (13) *d*-values for Cr_2O_3: 3.6310, 2.6650, 2.4800, 2.1752, 1.8152, 1.6724, 1.4649, 1.4316 Å). The highest intensity peak at a *d*-value of $d = 2.6650$ Å of Cr_2O_3 is masked by the second most intense peak of SnO_2 at $d = 2.6440$ Å, whereas the second highest intensity peak of Cr_2O_3 may be observed at $d = 2.4791$ Å . The third highest intensity peak of Cr_2O_3, $d = 1.6724$ Å, is again masked by SnO_2.

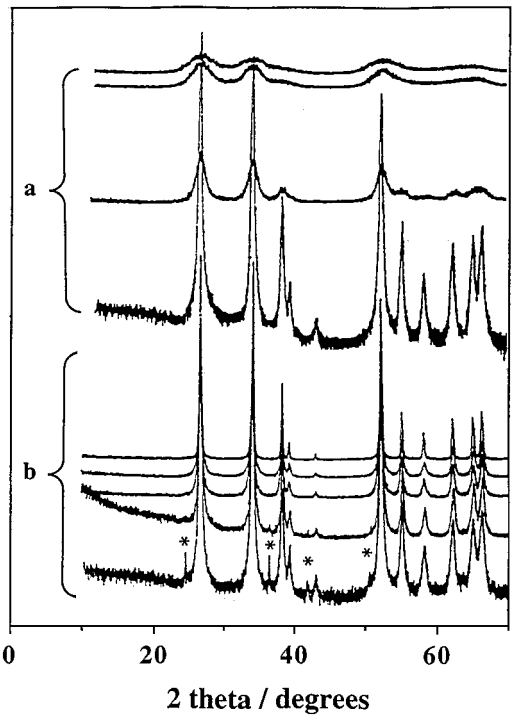

FIG. 5. The X-ray diffraction patterns of Cr(VI)/SnO_2 catalysts prepared by the gel impregnation route: (a) Diffractograms for the catalyst with a Cr : Sn ratio of 0.048 : 1 after calcination at temperatures of 333 (top), 573, 873, and 1273 K (bottom) and (b) diffractograms for catalysts with increasing chromium loadings after calcination at 1273 K (neat SnO_2 is shown as the top trace, with Cr : Sn ratios of 0.01, 0.048, 0.054, and 0.132 (bottom); peaks characteristic of Cr_2O_3 are denoted by asterisks).

TABLE 2

Average Particle Size (nm) of Cr(VI)/SnO_2 Materials Obtained by the Gel Impregnation Method Calculated from X-Ray Diffraction Peak Widths

		Calcination temperature (K)			
Cr : Sn Ratio	Phase	333	573	873	1273
0.011[a]	SnO_2	12	12	37	208
0.048[a]	SnO_2	12	12	34	408
0.054	SnO_2	12	—	37	136
	Cr_2O_3	—	—	—	63
0.132	SnO_2	12	12	39	204
	Cr_2O_3	—	—	—	139

[a] Cr_2O_3 not observed.

At higher chromium loadings (e.g., Cr : Sn 0.13), the chromium-containing phase becomes more pronounced with the peaks at $d = 2.6650$, 2.4791, and 3.6304 Å of Cr_2O_3 are now clearly observable beside the peaks at $d = 2.1765$, 1.8159, and 1.4638 Å. It is apparent that at chromium loadings of 0.054 and above, phase separation of Cr_2O_3 in Cr(VI)/SnO_2 catalyst materials is quite facile (Fig. 5b).

Transmission Electron Microscopy

TEM data were obtained for the La(III)/SnO_2 and the Cr(VI)/SnO_2 (obtained by the gel impregnation route, Cr : Sn 0.132) catalyst materials. Prior to any thermal treatment, the La(III)/SnO_2 catalyst material has a very similar appearance to other SnO_2-based catalyst materials (14, 15), the material being homogeneous with round 2- to 4-nm particles. However, profound changes occur upon calcination at 873 K, and three distinct phases are now observed. One has a La : Sn composition virtually identical to the material prior to calcination comprising small (ca. 4 nm) particles (Fig. 6, top left) and exhibits a weak electron diffraction pattern. The second component is lanthanum-rich and comprises particles of ca. 20 nm in size (Fig. 6, top middle), some of which are more electron dense than others and exhibit a crystalline electron diffraction pattern (Fig. 6, bottom middle). The third component is crystalline SnO_2 exhibiting a strong electron diffraction pattern (Fig. 6, bottom right). The same three components are also present after calcination at 1273 K, but now the SnO_2 is present as large (60 + nm) acicular lathes and rounded hexagons (Fig. 6, top right). The particle size of the lanthanum-rich phase has increased, and the phase which has evolved from the mixed Sn/La component now exhibits a strong electron diffraction pattern (Fig. 6, bottom left). These observations are totally consistent with the conclusions from XRD data, which indicated the development of the three phases SnO_2, La_2O_3, and $Sn_2La_2O_7$ corresponding to the three types of materials observed by TEM.

Micrographs of the Cr(VI)/SnO_2 (Cr : Sn 0.132) catalyst material obtained by the gel impregnation route show it to be remarkably similar. At room temperature the material comprises small (3–4 nm) homogeneous powder particulate (Fig. 7, top left and bottom left). Not much change occurs upon calcination at 573 K, although now a small number of distinct spots are superimposed on the powder electron diffraction pattern. By 873 K the particles have increased in size to ca. 10 nm and have the appearance of rounded hexagons, some of which appear more electron dense than others (Fig. 7, top middle), and the electron diffraction pattern (Fig. 7, bottom middle) exhibits a well developed spot pattern superimposed on the powder diffraction which is decreased relatively in intensity. By 1273 K the particulate comprises rounded hexagons, most of which are very electron dense (Fig. 7, top right), and the electron diffraction pattern is essentially that due to microcrystallites (Fig. 7, bottom right). Throughout the calcinations EDXA analysis showed that the Sn and Cr composition remains uniform.

Infrared and Raman Spectra

The infrared spectra of the Ln(III)/SnO_2 (Ln = La, Pr, Nd, Sm, Gd) catalyst materials prior to calcination and after calcination are all quite similar and exhibit the same general features as we have observed before for tin(IV) oxide gel itself (15). The spectra show that water is responsible for a large component of the unsymmetrical hydroxyl stretching envelope, while bands at 1144 and 1126 cm^{-1} are probably due to δ(OH) deformation modes of surface hydroxyl groups. Bands at 1379, 1333, 1084, 1033, and 830 cm^{-1} not observed in the spectra of tin(IV) oxide gel are probably due to adsorbed nitrate (16) which is not decomposed totally until high temperatures. The band at 610 cm^{-1} increases in intensity with increasing calcination temperature, and is assigned to the antisymmetric Sn–O–Sn stretching mode of a surface bridging oxide formed by condensation of adjacent surface hydroxyl groups (cf. ν_{as}(SnOSn) of $Me_3SnOSnMe_3$ (17), which occurs at 737 cm^{-1} and ν_{as}(SnOSn) of SnO_2 (15) which occurs at 770 cm^{-1}).

Infrared spectra for the Cr(VI)/SnO_2 (Cr : Sn 0.132) catalyst material obtained by the gel impregnation route before calcination exhibits features due to adsorbed water, surface hydroxyl groups and the bulk oxide are very similar to those observed in the spectra of the Ln(III)/SnO_2 (Ln = La, Pr, Nd, Sm, Gd) materials. However, substantial differences are apparent below ca. 1300 cm^{-1}. The bands at ca. 1245 and 1160 cm^{-1} are assigned to hydroxyl deformation modes of surface hydroxyl groups. These bands are lost after calcination at calcination temperatures of $\geq$873 K. The bands at ca. 942, 893, and 822(sh) cm^{-1} are assigned as Cr–O stretching modes of surface chromate species. These bands reduce in intensity on calcination but are still observable at 1273 K. The powder X-ray diffraction analysis shows the formation of Cr_2O_3 in this material at a calcination

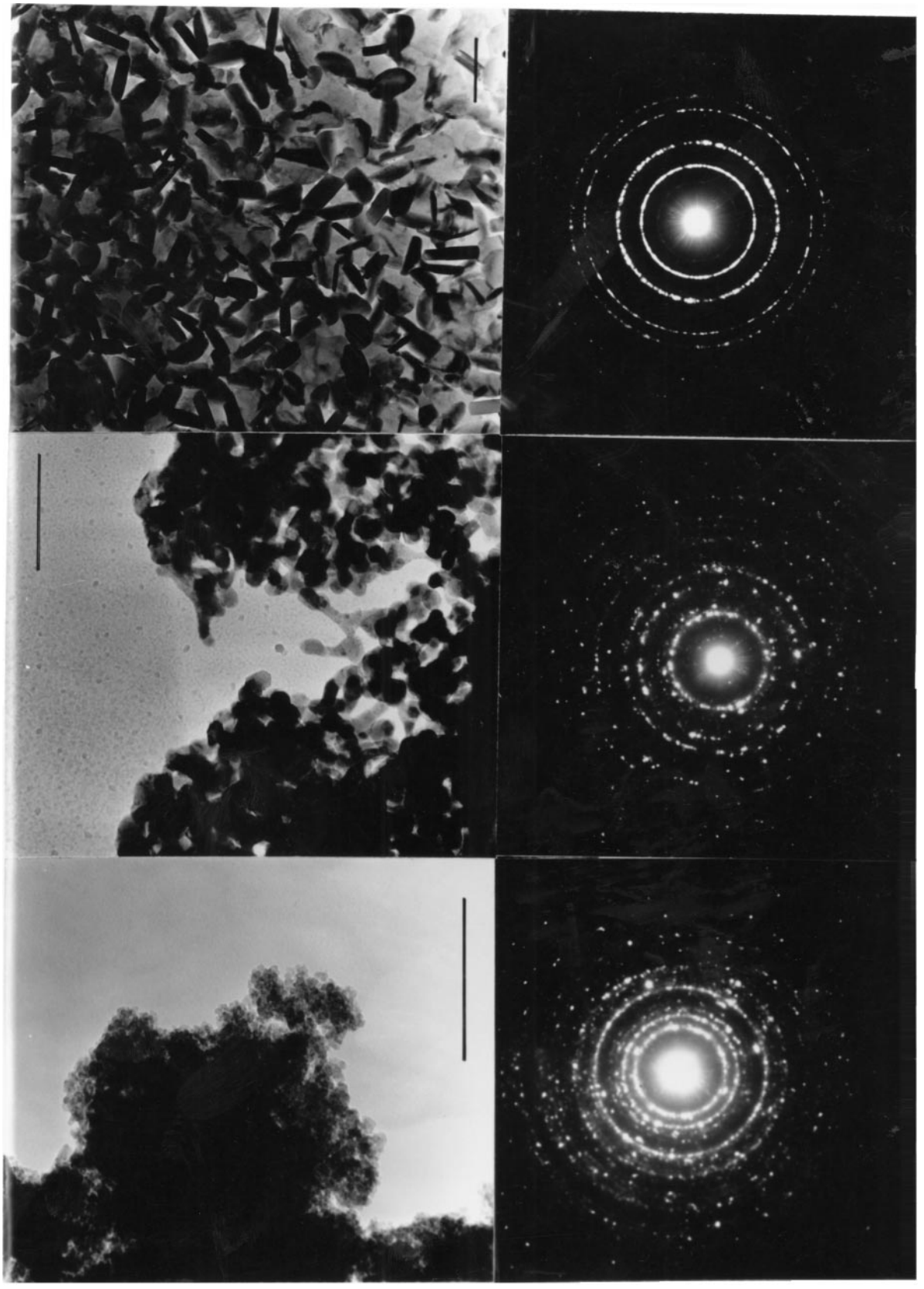

FIG. 6. (Top) Transmission electron micrographs of the La(III)/SnO_2 catalyst material (scale bars are all 100 nm); (bottom) associated electron diffraction patterns. See text for conditions and identification.

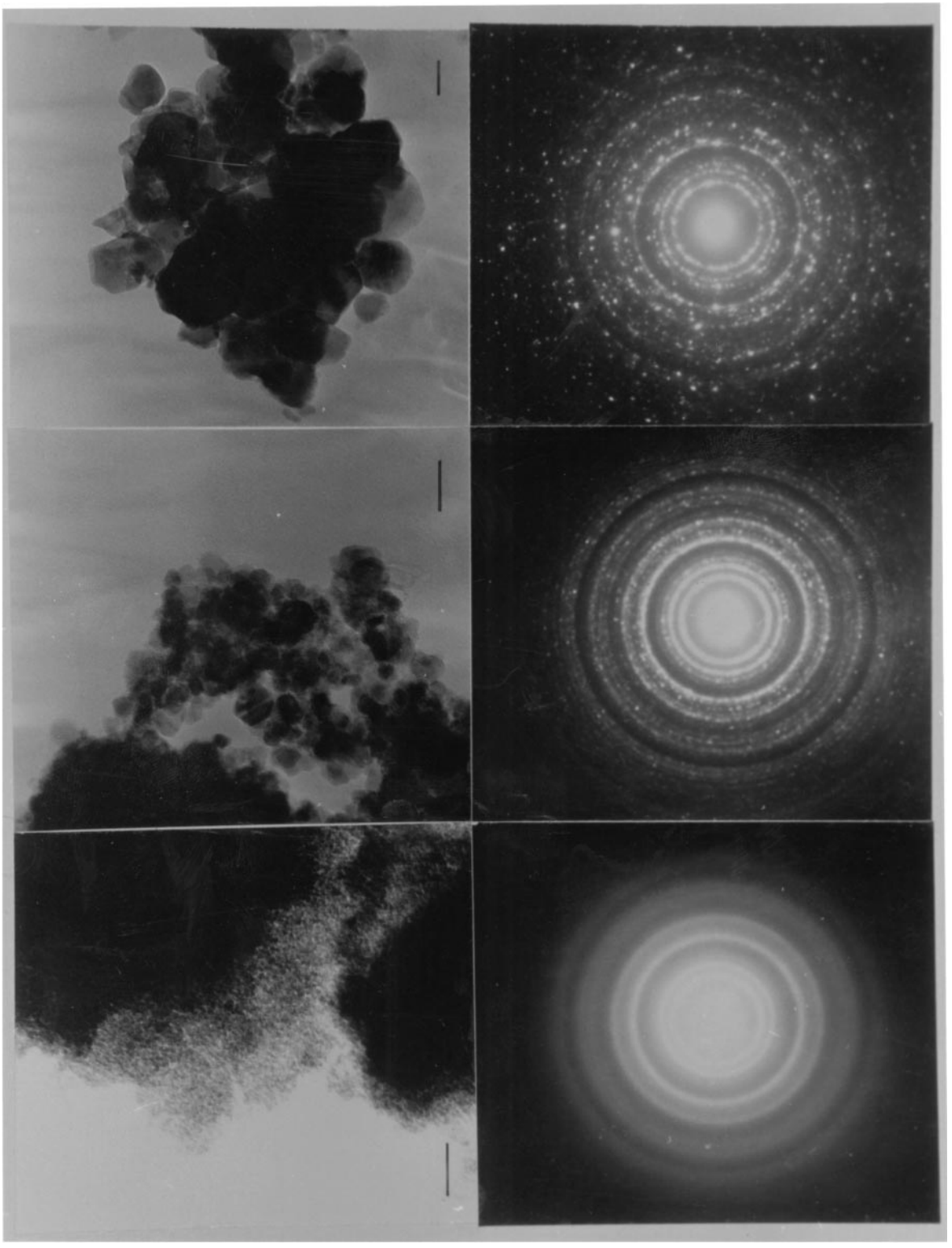

FIG. 7. (Top) Transmission electron micrographs of the Cr(VI)/SnO_2(Cr : Sn 0.132) obtained by the gel impregnation route (scale bars are 20 nm); (bottom) associated electron diffraction patterns. See text for conditions and identification.

TABLE 3

Observed Raman Bands for Chromate Anions in Aqueous Solution (cm^{-1}) (18–21)

CrO_4^{2-}	$Cr_2O_7^{2-}$	$Cr_3O_{10}^{2-}$	$Cr_4O_{13}^{2-}$	Assignment
		987*w*	987*w*	$\nu_{as}(CrO_2)$
		956*w*	963*m*	$\nu_s(CrO_2)$
886*w*	942*w*			$\nu_{as}(CrO_4)/(CrO_3)$
848*s*	904*s*	904*s*	902*m*	$\nu_s(CrO_4)/(CrO_3)$
		844*w*	842*m*	$\nu_{as}(Cr'OCr'')$

temperature of 1273 K, and it appears that the chromate(VI) species are transformed into Cr_2O_3 on calcination. As for the Ln(III)/SnO_2 materials, the intense broad band at ca. 610 cm^{-1} observed prior to calcination is assigned as the antisymmetric Sn–O–Sn stretching modes of the surface-bridging oxide formed by condensation of adjacent surface hydroxyl groups. The weak broad band observed at ca. 470 cm^{-1} is assigned to the symmetric Sn–O–Sn stretching mode (15).

More detail concerning the nature of the surface chromate species indicated in the infrared spectra may be gained from an examination of the corresponding Raman spectra. In aqueous solution (Table 3) CrO_4^{2-} ions exhibit two bands at 848 cm^{-1} (strong) and a much weaker band at 886 cm^{-1}, whereas the dichromate $Cr_2O_7^{2-}$ anion exhibits a strong band at 904 cm^{-1} and a weak band at 942 cm^{-1}. Higher polychromate anions such as $Cr_3O_{10}^{2-}$ and $Cr_4O_{13}^{2-}$ exhibit a greater number of bands in this region but, critically, have bands at higher wavenumber than do either mono- or dichromate ions. Therefore, the observation of bands at ca. 904 cm^{-1} and ca. 886 cm^{-1} may be used as diagnostic of mono- and dichromate species, respectively, while bands at >950 cm^{-1} are indicative of the presence of higher polychromate (tri- and/or tetrachromate) species.

The spectra of Cr(VI)/SnO_2 catalysts obtained by the gel impregnation route are similar in form in the range 750–1050 cm^{-1} (ν(Cr–O) region) irrespective of the Cr : Sn ratio, exhibiting two principal maxima together with several shoulders. However, the positions of the two peak maxima shift with the Cr : Sn ratio. When the chromium loading is very low (Cr : Sn 0.011), two broad weak bands at ca. 887 and 942 cm^{-1} are observed; the former indicates the presence of adsorbed CrO_4^{2-} ions while the latter indicates the presence of adsorbed $Cr_2O_7^{2-}$ anions (Table 3). Other bands due to these species are present as shoulder features, and it is also probable that the shoulder at high wavenumber is due to a small amount of $Cr_3O_{10}^{2-}$ anion. The vibration bands assigned for SnO_2 in this material exhibits only two large broad bands at ca. 632 and 475 cm^{-1}.

As the chromium loading is increased, the maxima shift to 886 and 942, 884, and 943, and 883, 895, and 949 cm^{-1} for Cr : Sn ratios of 0.048, 0.054, and 0.132, respectively. In all cases, pronounced shoulder features are present both to higher and lower wavenumber. The observed shift to higher wavenumber may be rationalized by an increased concentration of adsorbed $Cr_2O_7^{2-}$ and adsorbed $Cr_3O_{10}^{2-}$ anions in these catalysts as the concentration of the polyoxoanions increase in the aqueous CrO_3 solution. However, adsorbed CrO_4^{2-} ions could also be present but only in small amounts.

At higher loadings of chromium (Cr : Sn 0.054 and 0.132), besides exhibiting the two maximum vibrational bands of CrO_4^{2-} and $Cr_2O_7^{2-}$ anions and the strong shoulder features (ca. 973 and 981 cm^{-1}) of $Cr_3O_{10}^{2-}$ anions, the pair of bands at 846 and 853 cm^{-1} {ν_{as}(Cr–O–Cr)} and at 973 and 980 cm^{-1} {$\nu_s(CrO_2)$ and $\nu_{as}(CrO_3)$}, respectively, have become clearly resolved indicative of trimeric and tetranuclear oxochromium anions (19, 22–24). However, we cannot exclude other higher polychromate species at high Cr : Sn ratios. Another interesting feature to note is that, as the chromium loading is increased, the intensity of SnO_2 bands is reduced, indicating the increased coverage of the SnO_2 surface by adsorbed chromate ions.

When all these catalyst materials were calcined at 573 K, all the bands attributed to surface chromium disappear totally. The band at ca. 567 cm^{-1} which is assigned to SnO_2 can still be observed but at much reduced intensity. It is also interesting to point out that for the higher chromium loadings (above a loading of Cr : Sn 0.052) after calcination at 1073 K, the band at 550 cm^{-1} which is assigned to the metal–oxygen vibration of distorted octahedrally coordinated chromium(III) atoms (24) in crystalline Cr_2O_3 starts to appear. This Cr_2O_3 formation can also be observed from the XRD diffractogram (see above), but only after the catalyst has undergone calcination at 1273 K. This discrepancy between Raman and XRD data for the detection of Cr_2O_3 is due to the fact that crystallites must be larger than 40 Å to be detected by XRD; while Raman spectroscopy has excellent sensitivity to much smaller metal oxide crystallites. Thus, both the Raman and the XRD data reveal that Cr_2O_3 is formed in the material at higher calcination temperatures. The reason why the band at ca. 550 cm^{-1} is not observable for the sample of chromium loading below Cr : Sn 0.052 even after heat treatment at 1273 K is probably due to the very low chromium loading which give rise to highly dispersed, amorphous Cr_2O_3.

Gas Adsorption Data for Cr(VI)/SnO_2

Nitrogen adsorption isotherms for the Cr(VI)/SnO_2 (Cr : Sn 0.132) catalyst material obtained by the gel impregnation route at calcination temperatures up to 1273 K are shown in Fig. 8 with corresponding numerical data in Table 4. The freshly prepared material prior to calcination exhibits similar microporous properties to SnO_2 gel itself. However, on calcination, it becomes coarsely mesoporous at 873 K and at 1273 K becomes nonporous. At room temperature, the isotherm is characteristic of adsorption on a

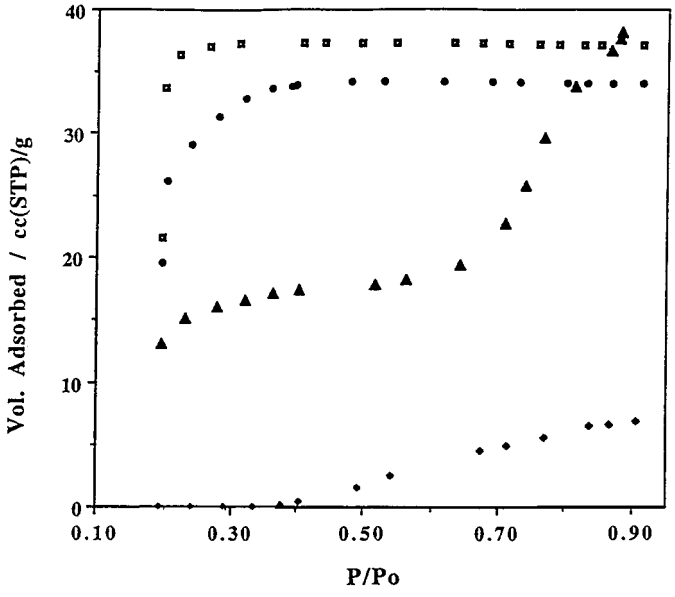

FIG. 8. Nitrogen adsorption isotherms for the Cr(VI)/SnO_2 oxide catalyst (Cr : Sn 0.132) obtained by the gel impregnation route after calcination at temperatures of 333 K (❐), 573 K (○), 873 K (▲), and 1273 K (◆).

microporous solid of Type I (Fig. 8) according to the BET classification (26). At 573 K the adsorption isotherm still retains Type I character but exhibits a lower gradient. At 873 K the adsorption isotherm is typical of Type IV behavior with coarse mesopore texture, but at 1273 K, the isotherm is that of a nonporous solid of Type III. Both isotherms of Types V and III are associated with weak adsorbent–adsorbate interactions. This weakness of the adsorbent–adsorbate forces cause the uptake at low relative pressure to be small but once a molecule has become adsorbed, the adsorbent–adsorbate forces promote the adsorption of further molecule by a cooperative process. This process rationalises the convexity of isotherms to the pressure axis at higher relative pressure (26).

From the BET isotherm, there is little doubt that the micropore filling process is responsible for the initial shape of the isotherm at low P/P_O at room temperature. The fairly high adsorption affinity, reflected by a steep uptake at low P/P_O, and the fairly high C value obtained, is a direct result of enhanced gas–solid interactions brought about by the close proximity of the gas molecules to pore walls in micropores (26).

Compared to SnO_2 gel which has a specific surface area (SSA) of ca. 185 $m^2\ g^{-1}$ decreasing to ca. 40 $m^2\ g^{-1}$ after calcination at 1273 K, the Cr(VI)/SnO_2 catalyst exhibits a much smaller SSA at room temperature (114 $m^2\ g^{-1}$), which is reduced by a relatively small amount to 96 $m^2\ g^{-1}$ on calcination at 573 K. However, after calcination at 1273 K the SSA is almost zero. This change is in accordance with the transformation of the microparticulate structure of the dried gel into a continuous dense oxide structure during the treatment, which results in progressive pore elimination. It has been shown that the surface properties of this type of oxide material change dramatically upon calcination at temperature >873 K. This behavior arises because densification at higher temperature eliminates most of the accessible pore surface, and changes the fairly highly porous structure to a dense and nonporous structure. However, the Cr(VI)/SnO_2 catalyst still seems to possess some external surface even after calcination at 1273 K as demonstrated by the existence of a small broad peak around 3400 cm^{-1} (ν(OH)) from infrared analysis (see above) due to hydroxyl species trapped in deep pores.

It is interesting to note that, although the surface area decreases dramatically with increasing temperature, there is only a small change in average pore size below 573 K compared to that above 573 K. When the Cr(VI)/SnO_2 gel is calcined up to 573 K agglomeration occurs and the pore volume decreases in proportion to the decrease in surface area while the pores which remain do not change much in size. It appears that portions of the gel agglomerate completely to a dense solid while the remainder undergoes little or no change. This behavior is similar to that of silica gel (27). However, above 573 K, the pore volume remains constant while the surface area decreases and the pore size increases. At 1273 K, the pore size is still the same as that at 873 K, but the pore volume is now severely reduced.

Comparing the data in Table 4, it is clear that calcination at 873 and 1273 K induces a large structural change in this type of catalyst. This is reflected by a large reduction in surface area and pore volume and a large increase in mean pore size. The small C value and zero micropore volume indicates that the sample calcined at 1273 K has lost its microporosity and has become a completely nonporous solid.

It has to be pointed out that a total elimination of surface Sn–OH and/or Cr–OH groups does not necessarily imply a total elimination of pores throughout the entire gel structure. Infrared data show that both the internal SnOH and/or CrOH groups have been found to exist in the sample

TABLE 4

BET Nitrogen Adsorption Data for the Cr(VI)/SnO_2 (Cr : Sn 0.132) Catalyst Prepared by the Gel Impregnation Method

Calcination temp (K)	V_m (cc/g)	A_{BET} (m^2/g)	C	V_p (cc/g)	d (Å)
333	26	114	167	0.057	18
573	22	96	425	0.053	19
873	13	58	16	0.059	40
1273	0.1	0.4	6	0.011	42

Note. V_m, monolayer capacity; A_{BET}, specific surface area derived from BET plot; C, BET constant; V_p, pore volume; d, mean pore diameter (calculated assuming that the samples contain cylindrical pores using the expression $d = 2(V_p)(A_S)^{-1} \times 10^4$) (25).

even after calcination at 1273 K, a result of hydroxyl species trapped in deep pores (pores with closed necks).

Density Measurements

The density of the Cr(VI)/SnO_2 (Cr : Sn 0.132) material obtained by the gel impregnation route measured using a conventional Weld pycnometer, increases with calcination temperature (Table 5). This distinct increase in density appears to be due to the formation of the crystalline phase of cassiterite (density 6.95 g cm^{-3} (29)), generated in the structure as shown by X-ray diffraction.

Increase in calcination temperature results in an increase in the density of the material and also in an increase of the average particle size of the sample. When comparing the average particle size from X-ray diffraction line broadening with the corresponding sizes obtained by nitrogen adsorption method (Table 5), it is obvious that the difference in size obtained by the two techniques is larger at higher calcination temperature. This phenomenon is mainly due to the low sensitivity of the line broadening technique to large crystallite sizes. Similar behavior has also been observed previously (30, 31) in the studies of Ag/α-Al_2O_3 catalysts.

MAS-NMR Spectra of the La(III)/SnO_2 Catalyst Material

The ^{119}Sn MAS-NMR spectra of the La(III)/SnO_2 catalyst material prior to and after calcination at 1373 K are shown in Fig. 9. The spectrum prior to calcination is complex and comprises a broad envelope covering ca. 200 ppm with a maximum centered at ca. −606 ppm and a shoulder at ca. −595 ppm. This spectrum is very similar to that of tin(IV) oxide gel itself and phosphorus- and silicon-modified tin(IV) oxide gels (14, 33). Tin(IV) oxide gel exhibits a broad envelope with a maximum also at ca. −606 ppm and a shoulder at ca. −587 ppm. The maximum is assigned to tin atoms incorporated into the SnO_2 lattice, while the latter are ascribed to tin atoms on the surface of the oxide particles and carrying hydroxyl groups.

TABLE 5

Comparison of the Average Particle Size (D) Obtained from Powder X-Ray Diffraction and Nitrogen Adsorption Methods for the Cr(VI)/SnO_2 (Cr : SN 0.132) Catalyst Prepared by the Gel Impregnation Method

Temp. (K)	Density (g cm^{-3})	$D_{X\text{-ray}}$[a] (Å)	D_{NA}[a] (Å)
333	4.15	117	115
873	5.42	382	187
1273	5.95	1361	1008

[a] $D_{X\text{-ray}}$ and D_{NA}, average particle size derived from X-ray diffraction and nitrogen adsorption methods, respectively, calculated using Eq. [29] $d = 6/\mu A_s$, where μ, density; A_s, specific surface area (derived from BET plots).

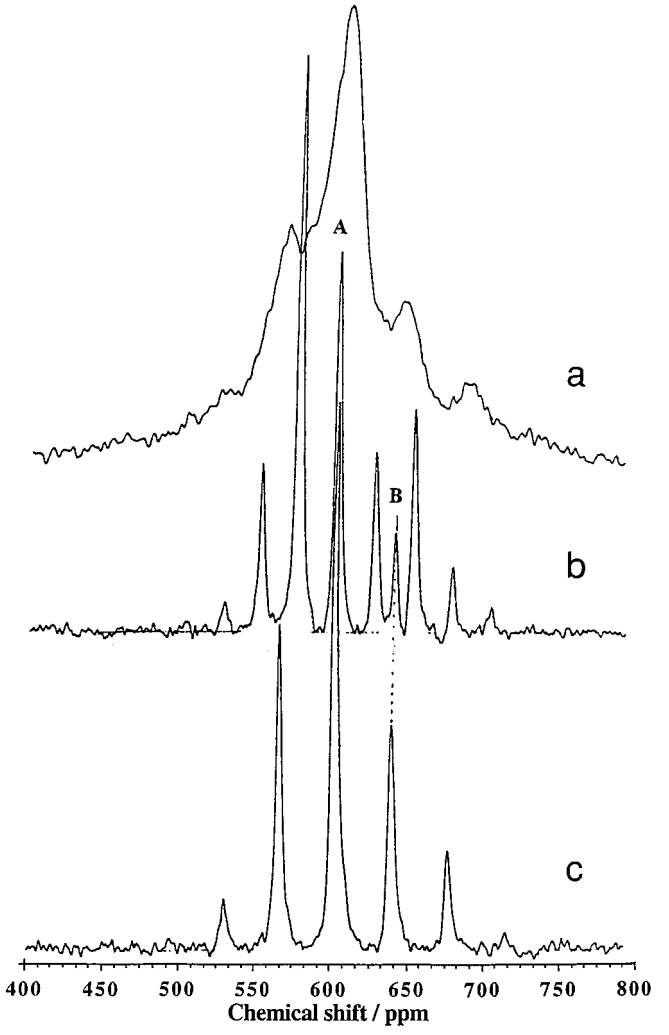

FIG. 9. ^{119}Sn MAS-NMR spectra of the La(III)/SnO_2 catalyst material recorded after drying at 333 K (spin rate 4320 Hz) (a) and after calcination at 1373 K (spin rate 2800 Hz (b); spin rate 4250 Hz (c)). The center bands for SnO_2 and $Sn_2La_2O_7$ are labeled A and B, respectively.

After calcination at 1373 K, the spectrum sharpens considerably and exhibits a resonance characteristic of crystalline SnO_2 with $\delta = -603.5$ ppm (cf. commercial tetragonal SnO_2 $\delta = -603.5$ ppm (33)) together with spinning sidebands. In addition, a new resonance is observed due to the ternary phase $Sn_2Ln_2O_7$ at $\delta = -641.6$ ppm (cf. lit. (34) $\delta = -642$ ppm).

DISCUSSION

Incorporation of lanthanide(III) or chromium(III) into tin(IV) oxide has little effect on the activity toward the catalytic oxidation of carbon monoxide, with complete conversion occurring by 560–613 K (cf. 615 K for SnO_2). However, chromium(III) does appear to have a promoting effect on tin(IV) oxide for the catalytic oxidation of propane

with complete conversion occurring in the temperature range 583–653 K depending on the Cr : Sn ratio in the catalyst. In contrast, catalytic oxidation of propane over the Ln(III)/SnO_2 materials is not complete until temperatures of ca. 740–750 K, similar to that of tin(IV) oxide itself.

Catalysts derived from tin(IV) oxide promoted using chromium(VI) sources exhibit activity which is dependent upon the Cr : Sn atomic ratio and the synthesis method. The most effective catalysts are produced by impregnation of tin(IV) oxide gel using aqueous chromium(VI) oxide solutions at a Cr : Sn ratio of 0.15 or treatment of tin(IV) oxide sol–gel using the same solution at a Cr : Sn ratio of 0.4. Both effect 100% CO conversion at ca. 510 K. The same catalysts are also the most effective for the conversion of propane, giving 100% conversion at ca. 560 K for both the gel- and the sol–gel-derived catalysts, a substantially lower temperature than for the Ln(III)/SnO_2 or tin(IV) oxide.

In comparison with a commercial Pt/Al_2O_3 catalyst, the most effective Cr(VI)/SnO_2 catalyst (e.g., sol–gel derived Cr : Sn 0.45) exhibits somewhat inferior activity for CO oxidation but significantly better activity toward propane oxidation. Although activity toward oxidation of CO is drastically affected by accelerated thermal aging of the catalyst, for propane oxidation the effect of accelerated aging is to decrease the activity of the Cr(VI)/SnO_2 catalyst to that of the commercial Pt/Al_2O_3 catalyst.

Thus it is apparent that Cr(VI)/SnO_2 catalysts are effective for the exhaustive oxidation of propane, comparing well with commercial noble metal catalysts. They also exhibit reasonable, but not exceptional, activity for the oxidation of carbon monoxide.

To attempt to rationalize the activity of catalysts derived by promotion of tin(IV) oxide using chromium(VI) compared to the much lower activity of Ln(III)/SnO_2 materials, we have carried out a preliminary examination of both types of material. Transmission electron microscopy shows that prior to calcination both types of material are homogeneous, comprising small (2–4 nm) particles of microcrystalline SnO_2 with the second dopant metal uniformly dispersed thoughout this particulate. Only relatively small increases in particle size occur on calcination to temperatures of ca. 873 K, but a rapid increase in size with temperature is observed thereafter. That no incorporation of heterometal ion into the SnO_2 lattice is observed to occur on calcination at high temperatures would indicate that prior to calcination the dopant metal ions are dispersed on the *surface* of the microcrystalline SnO_2 particulate. This conclusion is borne out for the Cr(VI)-doped tin(IV) oxide material where the vibrational spectra show the presence of adsorbed chromate anions.

After calcination at 1273 K, the pyrochlore $Sn_2Ln_2O_7$ phases and in some cases the La_2O_3 phase precipitates from the Ln(III)/SnO_2 materials, and Cr_2O_3 precipitates from the Cr(VI)/SnO_2 materials after calcination at 1273 K for materials with Cr : Sn atomic ratios $\geq$0.054. The formation of these phases probably occurs at significantly lower calcination temperatures, but X-ray diffraction is not sensitive enough for the detection of low levels of very small crystallites. Some corroboration of this for the La(III)/SnO_2 material comes from the transmission electron microscopic data in which three distinct phases are observed after calcination at 873 K. One has a La : Sn composition virtually identical to the material prior to calcination comprising small (ca. 4 nm) particles and exhibits a weak electron diffraction pattern. This we suggest is microcrystalline SnO_2 particulate, over the surface of which are dispersed La(III) cations. The second component is lanthanum-rich and appears to be microcrystallites of La_2O_3, while the third component is crystalline SnO_2.

Micrographs of the gel derived Cr(VI)/SnO_2 catalyst material show it to be remarkably similar, comprising microcrystalline SnO_2 particulate again with chromium species dispersed over the particulate surface for material calcined at temperatures up to 873 K. Throughout this temperature range the material remains homogeneous and no other phases are observed. It is very pertinent, however, to note that in the infrared the band at ca. 950 cm^{-1} still persists after calcination at temperatures $\leq$873 K, albeit reduced in intensity. This is indicative of the presence of some Cr(VI)=O functions, and it would appear that this is the principal difference in constitution between the Cr/SnO_2 and the Ln/SnO_2 materials.

That there is only a marginal difference in activity toward the oxidation of carbon monoxide between tin(IV) oxide itself and tin(IV) oxide doped with either chromium or lanthanides suggests that these modified materials are essentially unchanged in the context of CO oxidation. We have shown previously (35) that on copper(II)-promoted tin(IV) oxide the catalytic oxidation of carbon monoxide occurs by initial adsorption of CO at isolated or neighboring surface oxygen atoms to generate surface carboxylate or bidentate or bridging carbonate, followed by conversion of the species into unidentate carbonate and the desorption of carbon dioxide. The surface oxygen vacancies thus created are replenished by the dissociative chemisorption of dioxygen. The principal role of Cu(II) is mainly in electron transfer, i.e., it abstracts the negative surface charges (formed in the oxygen vacancies following desorption of CO_2) to form Cu(I), which is then oxidized back to Cu(II) by reaction with oxygen. It would appear in the present case that neither chromium nor lanthanide can facilitate this process, and hence neither can function as a promoter for the oxidation of CO.

The oxidation of propane must necesarily proceed by a different mechanism. We have demonstrated (36) that on PdO/SnO_2 and SiO_2/SnO_2 ethane adsorbs via hydrogen abstraction and subsequent oxidation of the surface ethoxide to a surface acetate, whereas no adsorption at all on tin(IV)

oxide itself occurs. The requirement in the catalyst to facilitate hydrogen abstraction is the presence of a basic surface oxygen species, and the remaining surface Cr(VI)=O functions after calcination at temperature up to 873 K are strong candidates for this role in the case of the $Cr(VI)/SnO_2$ catalyst materials.

Although these materials originate from chromium(VI) oxyanions of the types CrO_4^{2-}, $Cr_2O_7^{2-}$, and $Cr_3O_{10}^{2-}$ sorbed on to the surface of the tin(IV) oxide particles in the freshly prepared material, they are obviously not the chromium species which are present in the material after calcination at temperatures in the range 573–873 K. Candidates for the chromium species present in this temperature regime are lower oxides including Cr_3O_8, Cr_2O_5, Cr_5O_{12}, and CrO_2 which have been obtained by the thermal decomposition of CrO_3 (37).

The thermal decomposition behavior of CrO_3 supported on silica and alumina follows a broadly similar fashion as the unsupported compounds (38–40). Heating $Cr(VI)/SiO_2$ at 573 K affords poorly crystallized supported chromium oxides of stoichiometries $CrO_{2.1}$ and $CrO_{2.6}$, respectively, whereas at 873 K large crystallites of α-Cr_2O_3 are formed in both cases. The only effect of the silica support appears to be the formation of smaller chromium oxide particle sizes. No crystalline chromia species were formed on alumina as a support material irrespective of calcination temperature although very weak X-ray diffraction features of α-Cr_2O_3 are observed at 873 K. The stoichiometry of the chromium oxide species formed on alumina are independent of oxidation state of the chromium source and is determined only by the temperature of calcination, a stoichiometry of $CrO_{2.2}$ being formed at 573 K and $CrO_{1.7–1.8}$ being formed at 873 K. It would appear, therefore, that the predominant species formed on alumina after calcination at 573 K is chromium(IV) oxide, CrO_2.

Considering the quite different natures of silica and alumina as support materials on the one hand and tin(IV) oxide, it would be surprising if the same chromium oxide is generated on all, and hence further work to elucidate the nature of chromium species in these Cr/SnO_2 catalysts is in progress.

CONCLUSIONS

Catalysts obtained by calcination of chromium(VI)-promoted tin(IV) oxide at 573 K are effective for the oxidation of propane, affording 100% conversion at 553 K compared with ca. 700 K for a commercial Pt/Al_2O_3 catalyst. In contrast, similar $Ln(III)/SnO_2$ (Ln = La, Pr, Nd, Sm, Gd) materials show little enhancement in activity from SnO_2 itself.

ACKNOWLEDGMENTS

We thank the EPSRC (for Research Grant GR/J76026) for support and the Malaysian Government (for the award of a scholarship to W.A.).

REFERENCES

1. For the EC see EC Directives Dir. 88/76/EEC, December 1987, Dir. 88/436/EEC, 16 June 1988, and Dir. 89/458/EEC, 18 July 1989.
2. EC Communication COM (89) 662, 2nd February 1990.
3. Harrison, P. G., *in* "Chemistry of Tin" (P. G. Harrison, Ed.), Chap. 12. Blackie, Glasgow, 1989.
4. Fuller, M. J., and Warwick, M. E., *J. Catal.* **29**, 441 (1973).
5. Fuller, M. J., and Warwick, M. E., *J. Catal.* **34**, 445 (1974).
6. Bond, G. C., Molloy, L. R., and Fuller, M. J., *J. Chem. Soc. Chem. Commun.* 796 (1975).
7. Croft, G., and Fuller, M. J., *Nature* **269**, 585 (1977).
8. Fuller, M. J., and Warwick, M. E., *J. Catal.* **42**, 418 (1976).
9. Fuller, M. J., and Warwick, M. E., *Chem. Ind. (London)* 787 (1976).
10. Solymosi, F., and Kiss, J., *J. Catal.* **54**, 42 (1978).
11. Harrison, P. G., Azelee, W., Mubarak, A. T., Bailey, C., Daniell, W., and Lloyd, N. C., in "Catalysis and Automotive Pollution Control. IV. Studies in Surface Science and Catalysis" (N. Kruse, A. Frennet, and J.-M. Bastin, Eds.), Vol. 116. Elsevier, Amsterdam, 1998.
12. Louer, D., and Louer, M., *J. Appl. Crystallogr.* **5**, 271 (1972).
13. Powder Diffraction File, Inorganic Phases, International Centre for Diffraction Data, American Society of Testing Material, 1991.
14. Harrison, P. G., Perry, C. C., Creaser, D. A., and Li, X., *Eurogel'91*, 175 (1992).
15. Harrison, P. G., and Guest, A., *J. Chem. Soc. Faraday Trans. 1* **83**, 3383 (1987).
16. Ross, S. D., "Inorganic Infrared and Raman Spectra," pp. 154–158. McGraw-Hill, London, 1972.
17. Kriegsman, H., Hoffman, H., and Geissler, H., *Z. Anorg. Allg. Chem.* **341**, 24 (1965).
18. Gonzalez-Vilchez, F., and Griffith, W. P., *J. Chem. Soc. Dalton Trans.* 1417 (1972).
19. Vuurman, M. A., Ph.D thesis, Univ. of Amsterdam, 1992.
20. Michel, G., and Machiroux, R., *J. Raman Spectrosc.* **14**, 22 (1983).
21. Michel, G., and Machiroux, R., *J. Raman Spectrosc.* **17**, 79 (1986).
22. Hardcastle, F. D., and Wachs, I. E., *J. Mol. Catal.* **46**, 173 (1989).
23. Scharf, U., Schneider, H., Baiker, A., and Wokaun, A., *J. Catal.* **145**, 464 (1994).
24. Michel, G., and Cahay, R., *J. Raman Spectrosc.* **17**, 4 (1986).
25. Iler, R. K., "The Chemistry of Silica" Wiley, New York, 1979.
26. Bond, G. C., "Heterogeneous Catalysis Principles and Applications," 2nd ed. Academic Press, London, 1987.
27. Brunauer, S., Deming, L. S., Deming, W. S., and Teller, E., *J. Am. Chem. Soc.* **62**, 1723 (1940).
28. Gregg, S. J., and Sing, K. S. W., "Adsorption, Surface Area and Porosity," 2nd ed. Academic Press, London, 1982.
29. Gregg, S. J., and Sing, K. S. W., "Adsorption, Surface Area and Porosity," 2nd ed. Academic Press, London, 1982.
30. Yu Gavrilov, V., and Zenkovets, G. A., *J. Catal.* in communication, 1994.
31. Arohmayer, D. E., Geoffrey, G. L., and Vannice, M. A., *Appl. Catal.* **7**, 189 (1983).
32. Gavriilidis, A., Sinno, B., and Varma, A., *J. Catal.* **139**, 41 (1993).
33. Harrison, P. G., *Catal. Today* **17**, 483 (1993).
34. Grey, C. P., Dobson, C. M., and Cheetham, A. K., *J. Am. Chem. Soc.* **111**, 505 (1989).
35. Harrison, P. G., and Maunders, B., *J. Chem. Soc. Faraday Trans. I* **81**, 1311 (1985).
36. Zhao, D., Shane, J. J., Daniell, W., Harrison, P. G., and Goldfarb, D., *J. Appl. Mag. Reson.* **10**, 539–557 (1996).
37. Wilmhelmi, K. A., *Acta Chem. Scand.* **19**, 165 (1965).
38. Fouad, N. E., Knozinger, H., and Zaki, M. I., *Z. Phys. Chem.* **186**, 231 (1994).
39. Fouad, N. E., Knozinger, H., Ismail, H. M., and Zaki, M. I., *Z. Phys. Chem.* **173**, 201 (1991).
40. Fouad, N. E., Knozinger, H., Zaki, M. I., and Mansour, S. A. A., *Z. Phys. Chem.* **181**, 75 (1991).